Applied Catalysis B: Environmental 179 (2015) 220–228

Contents lists available at ScienceDirect

Applied Catalysis B: Environmental

journal homepage: www.elsevier.com/locate/apcatb

Fabrication of novel heterostructured few layered WS_2-Bi_2WO_6/$Bi_{3.84}W_{0.16}O_{6.24}$ composites with enhanced photocatalytic performance

Jian-Ping Zou[a], Jun Ma[a], Jin-Ming Luo[b], Jian Yu[a], Junkai He[c], Yongtao Meng[c], Zhu Luo[c], Shao-Kui Bao[a], Hui-Long Liu[a], Sheng-Lian Luo[a,*], Xu-Biao Luo[a], Tong-Cai Chen[a], Steven L. Suib[c,*]

[a] Key Laboratory of Jiangxi Province for Persistent Pollutants Control and Resources Recycle, Nanchang Hangkong University, Nanchang, Jiangxi, China
[b] Key Laboratory of Drinking Water Science and Technology, Research Center for Eco-Environmental Sciences, Chinese Academy of Sciences, Beijing, China
[c] Department of Chemistry, University of Connecticut, Storrs, CT, USA

ARTICLE INFO

Article history:
Received 28 September 2014
Received in revised form 12 April 2015
Accepted 12 May 2015
Available online 14 May 2015

Keywords:
Bismuth tungstates
Few layered WS_2
Heterostructured
Photocatalysis
Transition metal dichalcogenides

ABSTRACT

Novel heterostructured composite of few layered WS_2-Bi_2WO_6/$Bi_{3.84}W_{0.16}O_{6.24}$ has been synthesized via a facile hydrothermal method for the first time. The obtained catalysts were systematically characterized by X-ray diffraction (XRD), SEM, TEM, EDS, Raman spectroscopy, atomic force microscopy (AFM), X-ray photoelectron spectroscopy (XPS) to certify the existence of WS_2 with a few-layered structure among the heterostructured composite, and to illuminate the relationship of its performance and the structural features. Among the as-prepared catalysts, the few layered WS_2-Bi_2WO_6/$Bi_{3.84}W_{0.16}O_{6.24}$ composite show the best photocatalytic degradation of RhB under visible light irradiation. The enhanced photocatalytic performance of the heterostructured few layered WS_2-Bi_2WO_6/$Bi_{3.84}W_{0.16}O_{6.24}$ composite is attributed to the two-dimensional structure of WS_2 with special properties and the matching energy band structure for efficient separation of photogenerated electron–hole pairs. The formation mechanism and photocatalytic mechanism were proposed. The present work firstly combined layered TMDs with composites to prepare ternary heterostructured catalysts, which provide new ideas for obtaining novel layered TMDs-based composites with excellent performance.

1. Introduction

Recently, tremendous attention has been paid to graphene, a two-dimensional and single-layer carbon material with various fascinating properties, which are mainly due to its atomic-layer thickness and 2D morphology [1,2]. Similar to the case of graphene, layered graphene-like materials have received considerable interest, such as transition metal dichalcogenides (TMDs) [3–6]. TMDs with band gaps of 1.0–2.0 eV consist of a hexagonal layer of metal atoms (W or Mo) that is sandwiched between two layers of chalcogen atoms. And then the hexagonal layers of metal atoms combine with the layers of chalcogen atoms via from bulk to a few layers of sheets, some remarkable changes and layer-dependent properties are revealed, such as the improvement of photoluminescence and the transformation from indirect to a direct bandgap as a 2D semiconductor, which are all attributed to quantum confinement and surface effects [7–12].

Up to now, the layered TMDs, such as MoS_2, $MoSe_2$, and WS_2, have been investigated and employed in a wide range of applications, such as lithium ion batteries, solid lubricants, field effect transistor (FET), and supercapacitors [13–16]. Meanwhile, the layered TMDs are known as efficient electrocatalysts and photocatalysts for the hydrogen evolution reaction (HER). For example, WS_2 nanosheets obtained through chemically exfoliation and solid state methods show an enhanced electocatalytic activity for HER [17,18]; limited-layer MoS_2-graphene hybrids can improve the efficiency of the photocatalytic HER [19]; MoS_2/graphene-TiO_2 exhibits much better photocatalytic H_2 production activity compared with pure TiO_2 [20]. However, related research is mainly focused on the combination with some simple compounds (such as carbon materials, metal oxides or sulfides and so on) but rarely involved in the design and preparation of layered TMDs-based composites containing metal oxysalts or other complex compounds.

* Corresponding authors. Tel.: +86 791 83863688 / +1 860 4862797; fax: +86 791 83953373/ +1 860 4862981
E-mail addresses: sllou@hnu.edu.cn (J. Ma), sllou@hnu.edu.cn (S.-L. Luo), steven.suib@uconn.edu (S.L. Suib).

http://dx.doi.org/10.1016/j.apcatb.2015.05.031
0926-3373/

Bismuth tungstate is one of the simplest and mostly studied aurivillius oxides, which has been demonstrated to be a good visible-light-active photocatalyst with unique properties [21,22]. Till now, many studies have been carried out to clarify the relationship between morphologies and activities of bismuth tungstate [23–27], as well as preparation of novel heterostructured composites with good photocatalytic performance via coupling bismuth tungstate with many semiconductors and carbon materials, such as TiO_2 [28], Bi_2O_3 [29], Bi_2S_3 [30], Co_3O_4 [31], $PtCl_4$ [32], graphene [33,34], and so on. However, investigations of heterostructured composites containing bismuth tungstate with two mixed phases are rare, which has attracted extensive attention in anatase/rutile TiO_2 [35,36], $WO_3/WO_3{\cdot}H_2O$ [37], $Bi_2MoO_6/Bi_{3.64}Mo_{0.36}O_{6.55}$ [38,39], $In_2O_3/In_2O_3{\cdot}3H_2O$ [40], and α-Ga_2O_3/β-Ga_2O_3 [41] composites. The coupling of polymorphs of crystalline phases can always build a matching energy band structure for the effective suppression of charge recombination, and contribute to design of more complicated multi-functional materials. Meanwhile, with a view to the outstanding performance of graphene/Bi_2WO_6 composites [33,34], designed composites of mixed-phase bismuth tungstate decorated by 2D graphene-like TMDs seem to be relatively unexplored.

In addition, the 2D structural TMDs (MX_2) nanosheets have high surface energy and native vacancy defects (X and M single vacancies, X_2 and MX double vacancies, and MX_2 triple vacancies), and their colloidal dispersions are all negatively charged with a negative zeta potential. This feature of the layered TMDs allows interaction with cations and provides reactive sites for the nucleation and growth of nanomaterials. Herein, we make full use of the features of layered WS_2 and combine the few layered WS_2 with $Bi_2WO_6/Bi_{3.84}W_{0.16}O_{6.24}$ composites to prepare a novel few-layer WS_2-$Bi_2WO_6/Bi_{3.84}W_{0.16}O_{6.24}$ heterostructured composite via in situ hydrothermal reaction. Due to the special properties of the few layered WS_2, the separation of the photogenerated electrons and holes is enhanced as well as the transport rate of photocarriers. Thus, an improvement of photocatalytic efficiency is achieved over WS_2-$Bi_2WO_6/Bi_{3.84}W_{0.16}O_{6.24}$ composites. The possible formation and photocatalytic mechanisms of the materials were proposed. The present investigation not only provides a facile method to prepare a novel ternary heterostructured photocatalyst but also promotes our in-depth thinking on designing and fabricating novel layered TMDs based composites for photocatalysis and other technological applications.

2. Experimental

2.1. Materials and syntheses

2.1.1. Preparation of Liquid exfoliation of few layered WS_2

All chemicals were AR grade and used without further purification. Bulk WS_2 powder (1.5 g, 1–6 μm, Aladdin Reagent Inc.,) was added into a 500 mL flask. *N*-methyl-2-pyrrolidone (300 mL) was added as dispersion solvent. The sealed flask was sonicated for 48 h in a sonic bath (40 kHz, 150 W, KQ3200DB, Kun Shan Ultrasonic Instruments Co., Ltd). Following the established procedure [42], the dispersion was centrifuged at 500 rpm for 15 min to remove sediment. The supernatant was collected and treated by reduced pressure distillation. The obtained solid was washed with ethanol and deionized water for several times, and then dried in a vacuum freeze drier for 72 h.

2.1.2. Preparation of the WS_2-$Bi_2WO_6/Bi_{3.84}W_{0.16}O_{6.24}$ photocatalyst

The obtained few-layered WS_2 (30 mg) was dispersed in a solution of 30 mL deionized water and 10 mL ethanol with ultrasonication for 30 min. $Bi(NO_3)_3{\cdot}5H_2O$ (0.86 mmol) was dissolved in 5 mL 1 M HNO_3 solution and the solution was slowly added to the WS_2 solution under stirring for 3 h. Then a stoichiometric amount of $Na_2WO_4{\cdot}2H_2O$ (0.43 mmol) was dissolved in 5 mL deionized water, and slowly dropped into the above solution. Subsequently, the pH of the mixed solution was adjusted by adding NaOH solution to a designed value (pH 0.5). After stirring for 1 h at room temperature, the mixture was transferred into a 100 mL Teflon-lined stainless steel autoclave up to 80% of the total volume. The autoclave was heated at 150 °C for 3 h, and then cooled to room temperature. The resulting solid was recovered by filtration, washed with deionized water and ethanol several times, and then dried at 60 °C for 24 h. The obtained dark powder was WS_2-$Bi_2WO_6/Bi_{3.84}W_{0.16}O_{6.24}$ and labeled WS_2-BWO. For comparison, pure $Bi_2WO_6/Bi_{3.84}W_{0.16}O_{6.24}$ (noted as BWO) and WS_2 (bulk)-$Bi_2WO_6/Bi_{3.84}W_{0.16}O_{6.24}$ (noted as (B)WS_2-BWO) were also prepared by the hydrothermal method under the same conditions as mentioned above without the few layered WS_2 and with the same amount of bulk WS_2, respectively. Bi_2WO_6 and $Bi_{3.84}W_{0.16}O_{6.24}$ were prepared at a pH 9 and 11, respectively, and the other conditions are the same as those of the synthesis of $Bi_2WO_6/Bi_{3.84}W_{0.16}O_{6.24}$.

2.2. Characterization

The crystalline phases of samples were collected on a Bruker D8 Advance X-ray diffractometer (Cu-Kα radiation, λ = 1.5406 Å in a 2θ range from 10° to 70° at room temperature with a scanning speed of 2°/min). The morphologies of the as-prepared samples were examined by a field-emission scanning electron microscope (SEM, FEI, Holland) and a transmission electron microscope (JEM-2010HR). Composition analyses on the samples of as-prepared catalysts were performed on a field-emission scanning electron microscope equipped with an energy dispersive X-ray spectroscope (EDS). X-ray photoelectron spectroscopy (XPS) measurements were taken with a VG Escalab 250 spectrometer equipped with an Al anode (Al-*Kα* = 1486.7 eV). Raman spectra were recorded on a microscopic confocal Raman spectrometer (JY LabRam HR800) with a laser source of 785 nm for excitation. The optical property was analyzed by both UV–VIS–NIR diffuse reflectance spectra (DRS, Varian Cary 300) and photoluminescence spectra (F-7000, Hitachi, Japan) at room temperature. Zeta potentials were analyzed with a Zetasizer Nano-ZS90 (Malvern). The Brunauer–Emmett–Teller (BET) surface areas of samples were measured by means of N_2 adsorption over a NOVA 2000e (Quantachrome) equipment.

2.3. Electrochemical measurements

Electrochemical measurements were performed on a CHI 660D electrochemical workstation (Shanghai Chenhua, China) using a standard three-electrode cell with a working electrode, a graphite electrode as counter electrode, and a standard calomel electrode in saturated KCl as reference electrode. The working electrodes were prepared by dip-coating: 20 mg of photocatalyst was suspended in 5 mL ethanol to produce a slurry that was then dip-coated onto a 2 cm × 0.5 cm fluorine-tin oxide (FTO) glass electrode with a sheet resistance of 15 Ω. After drying under ambient condition, the films were sintered at 300 °C for 1 h. The electrolyte (0.5 M K_2SO_4 aqueous solution) was purged with nitrogen. The flatband potentials (V_{fb}) were determined from Mott–Schottky plots by electrochemical methods. The electrochemical impedance spectroscopic (EIS) investigation was carried out at open circuit potential in the presence of a 2.5 mM $K_3[Fe(SCN)_6]/K_4[Fe(SCN)_6]$ (1:1) mixture (as a redox probe) in 0.5 M K_2SO_4 aqueous solution. As for photocurrent measurements, a 300 W xenon lamp was used to generate visible light (with a 420 nm cutoff filter) and the other conditions were similar to those of electrochemical measurements.

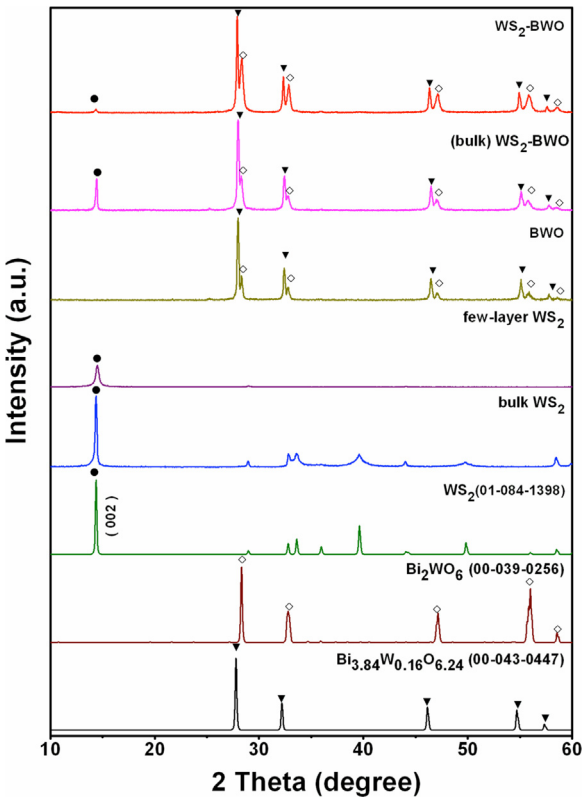

Fig. 1. XRD patterns of as-prepared samples of bulk WS_2, few-layer WS_2, BWO, and WS_2-BWO.

2.4. Photocatalytic experiment

Photocatalytic activities of the samples were evaluated by the photocatalytic degradation of rhodamine B (RhB) under visible light. A 300 W Xe lamp (PerfectLight, wavelength range: 320 nm ≤ λ ≤ 780 nm, light intensity: 160 mW/cm^2) was used as the light source with a 420 nm cutoff filter to provide visible-light irradiation. For the degradation of RhB, 100 mg of samples were added into 100 mL of RhB solution (10^{-5} M) under the irradiation of visible light. Before illumination, the solution was stirred for 1 h in the dark in order to reach the adsorption-desorption equilibrium between the photocatalyst and RhB. At 10 min intervals, a 5 mL solution was sampled. Then the concentration of RhB was detected by recording the absorbance at the characteristic band of 553 nm using a Hitachi U-3900H UV–visible spectrophotometer.

3. Results and discussion

3.1. Characterization of as-prepared samples

As shown in Fig. 1, compared with the pattern of bulk WS_2, the exfoliated few-layered WS_2 only possesses a broad and weak (0 0 2) diffraction peak, which is attributed to the destruction of van der Waals interactions between adjacent nanosheets [5,43–45]. And the BET results show that the surface area of WS_2 became twice as much after exfoliation. (Fig. S1). These results demonstrate that the bulk WS_2 was successfully exfoliated to a few layered structure. In addition, as shown in Fig. 1, the as-prepared bismuth tungstate composite at pH of 10.5 consists of two mixed phases of Bi_2WO_6 (JCPDS No. 00-039-0256) and $Bi_{3.84}W_{0.16}O_{6.24}$ (JCPDS No. 00-043-0047). In the pattern of the heterostructured WS_2-BWO composite, there are obvious characteristic peaks of BWO and a weak diffraction peak (0 0 2) of the few layered WS_2. Compared with the diffraction peaks of bulk WS_2 and the few layered WS_2, those of the few layered WS_2 among the WS_2-BWO composite evidently weaken. This phenomenon can be explained by the bismuth tungstate phases effectively suppressing the re-stacking of exfoliated WS_2 and are closely bonded with the few layered WS_2.

Fig. 2a–f show the scanning electron microscopy (SEM) images of as-prepared samples. Bulk WS_2 possesses an average diameter of ~5 μm and a thickness of ~100 nm (Fig. 2a). After ultrasonic exfoliating, the bulk structure transforms into nanosheets with an average diameter of about 500 nm (Figs. 2b and S2). Bi_2WO_6 exhibits a similar morphology to that of the few layered WS_2 (Figs. 2c and S2). As shown in Figs. 2d and S2, the $Bi_{3.84}W_{0.16}O_{6.24}$ phase possesses a blocky morphology with an average diameter of 50–100 nm. Fig. 2e shows that the morphology of BWO consists of nanosheets and nanospheres, corresponding to Bi_2WO_6 and $Bi_{3.84}W_{0.16}O_{6.24}$ in the BWO composite, respectively. As for the heterostructured WS_2-BWO, the nanoparticles ($Bi_{3.84}W_{0.16}O_{6.24}$) with uniform size evenly distribute on the nanosheets (Bi_2WO_6 and the few-layered WS_2) and contact with each other closely (Fig. 2f). The co-presence of nanoparticles and nanosheets can be obviously observed in the TEM images of WS_2-BWO (Figs. 3a–c). The EDS analysis of the selected field with two morphologies reveals that the existence of Bi, W, O, S elements is attributed to Bi_2WO_6, $Bi_{3.84}W_{0.16}O_{6.24}$ and WS_2, and the formation of heterojunctions between different phases is achieved.

To check the elemental composition of the WS_2-BWO composite, X-ray photoelectron spectroscopy (XPS) was employed. The results are shown in Fig. 4. All binding energies are calibrated using the C 1s peak at 284.6 eV. As displayed in Fig. 4a, the characteristic binding energy values of 158.7 and 164 eV for Bi $4f_{7/2}$ and Bi $4f_{5/2}$ reveal a trivalent oxidation state for bismuth in B_2WO_6 and $Bi_{3.84}W_{0.16}O_{6.24}$ [46,47]. As shown in Fig. 4b, the binding energies of 32.4 and 34.9 eV for W $4_{f7/2}$ and W $4f_{5/2}$ peaks are attributed to W^{4+} in WS_2, while the peak of 37.5 eV is due to W^{6+} in Bi_2WO_6 and $Bi_{3.84}W_{0.16}O_{6.24}$ [47,48]. The S 2p binding energies 161.8 eV (S $2p_{3/2}$) and 164.1 eV (S $2p_{1/2}$) in WS_2, and the O 1s binding energy 530.1 eV (crystal lattice oxygen) are also identified in the spectra (Fig. 4c and d) [48,49]. These results show evidence for the presence of WS_2 in the ternary heterostructured WS_2-BWO composite.

Raman spectra can be used to identify layered compounds [50–52]. The as-prepared samples were characterized by Raman spectroscopy. As shown in Fig. 5a, compared to the narrow bands at 355 (E_{2g}) and 419.8 cm^{-1} (A_{1g}) of bulk WS_2 with FWHM values around 5.4 and 5.3 cm^{-1}, respectively, the spectrum of the few layered WS_2 obtained by liquid exfoliation shows bands at 356.4 and 413.6 cm^{-1} with FWHM values of 7.8 and 7.6 cm^{-1}, respectively. The shifts of a few wavenumbers and widening of bands after exfoliation demonstrate the successful exfoliation from the bulk structure to a few layers [53,54]. Furthermore, the Raman spectra of the few layered WS_2, BWO and WS_2-BWO are displayed in Fig. 5b. The Raman peaks of BWO mainly appear in the range of 100–300 cm^{-1} and are assigned to the vibrational mode of Bi-O and WO_4, and 600–900 cm^{-1} assigned to the antisymmetric bridging mode (719 cm^{-1}), antisymmetric/symmetric A_g modes of the terminal O-W-O (796 and 825 cm^{-1}, respectively) [55–57]. By comparison, the Raman spectra of WS_2-BWO present the characteristic peaks of WS_2 and BWO but show a slight difference from those of pure WS_2 and BWO, which reveals the formation of a heterostructure between WS_2 and BWO in the WS_2-BWO composite.

The optical property of the as-prepared WS_2-BWO composite is also investigated through UV–vis diffuse reflectance spectra (DRS). As shown in Fig. 6a, the WS_2-BWO composite exhibits enhanced absorption intensity in the visible region and the absorption edge occurs a significant red-shift to 510 nm compared with BWO, Bi_2WO_6, and $Bi_{3.84}W_{0.16}O_{6.24}$. These may be attributed to the

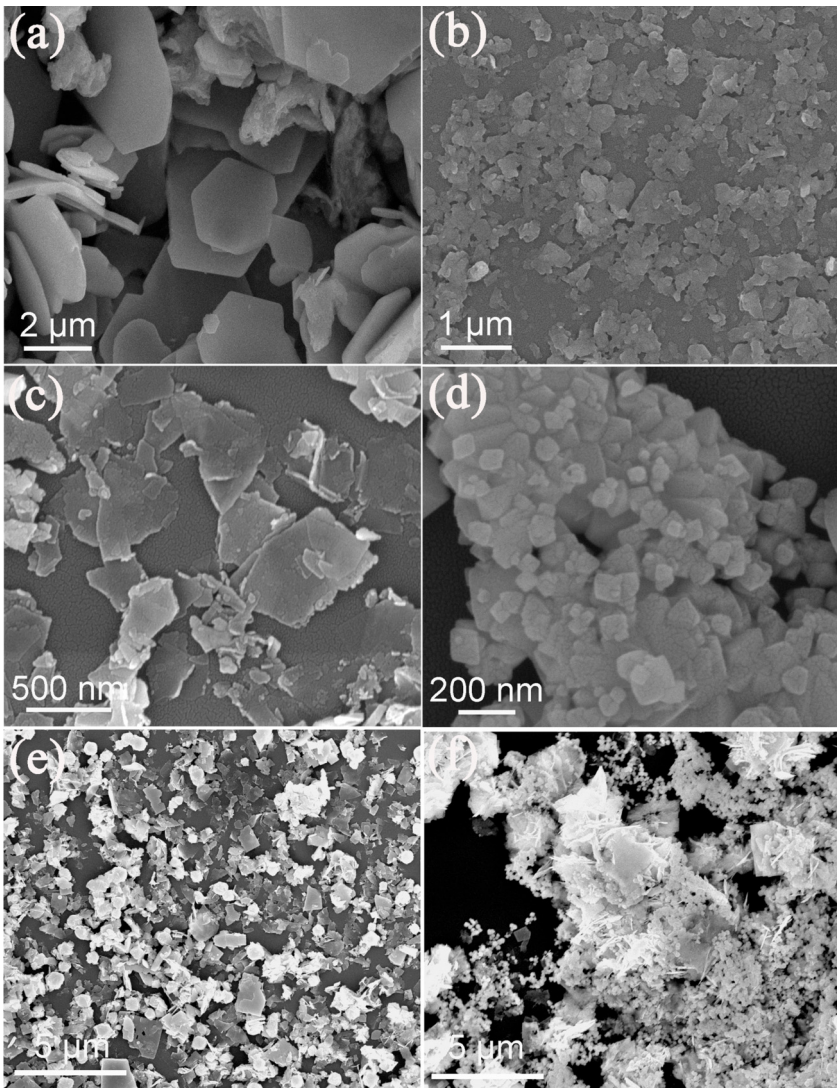

Fig. 2. SEM images of (a) bulk WS_2, (b) few-layer WS_2, (c) Bi_2WO_6, (d) $Bi_{3.84}W_{0.16}O_{6.24}$, (e) BWO, and (f) the heterostructured WS_2-BWO samples.

coupling of the few layered WS_2 and BWO, which is conducive to the enhancement of photocatalytic performance.

In order to investigate the recombination of photo-induced electrons and holes, the photoluminescence (PL) spectra of the as-prepared samples are measured. As shown in Fig. 6b, all three samples exhibit similar peak shapes and peak positions under the excited wave length of 300 nm, while the intensities of peaks are different. With the introduction of WS_2, the PL intensities of the peaks are obviously lower than that of pure BWO, indicating that the heterojunctions can suppress the recombination of photogenerated electrons and holes. In addition, the WS_2-BWO shows the lowest PL intensity, suggesting the highest separation efficiency of photo-induced electrons and holes, which is attributed to the special properties of the few layered structure of WS_2.

3.2. Formation mechanism

A possible formation mechanism of the WS_2-BWO is proposed for the first time as shown in Scheme 1. Firstly, the bulk WS_2 is ultrasonic in NMP solvent via a liquid exfoliation method, then transforms to the few layered WS_2 nanosheets with negative zeta potential (Fig. S3) and native vacancy defects (S and W single vacancies, S_2 and WS double vacancies, and WS_2 triple vacancies) [58] When the Bi^{3+} ion is added into the few layered WS_2 aqueous dispersion, Bi^{3+} ions interact electrostatically with WS_2 nanosheets and adsorb preferentially on the vacancies to form Bi^{3+}-WS_2 complexes. In the following hydrothermal process, these Bi^{3+}-WS_2 complexes react with the WO_4^{2-} at a certain pH value to generate the bismuth tungstate seed particles, and then form the Bi_2WO_6 nanosheets and $Bi_{3.84}W_{0.16}O_{6.24}$ nanoparticles in situ on the WS_2 nanosheets. Finally, the heterostructured WS_2-Bi_2WO_6/$Bi_{3.84}W_{0.16}O_{6.24}$ composite (WS_2-BWO) was obtained. Due to the existence of the few layered WS_2, the sizes and distribution of the $Bi_{3.84}W_{0.16}O_{6.24}$ nanoparticles and Bi_2WO_6 nanosheets become more uniform, which may be a reason for the enhancement of their photocatalytic activity.

In addition, as for the formation of BWO composite, pH value is a key factor to form two phased bismuth tungstate. There are two different products during the reaction with different pH values. And the reaction is illustrated as below:

$$Bi(NO_3)_3 + H_2O \rightarrow BiONO_3 + 2H^+ + 2NO_3^- \quad (1)$$

$$BiONO_3 + H_2O \rightarrow Bi_2O_2(OH)NO_3 + H^+ + NO_3^- \quad (2)$$

When the pH value is lower than that of 10.5, WO_4^{2-} will react with H^+ to form H_2WO_4. The relevant chemical reaction for Bi_2WO_6 can be formulated as follows:

$$Bi_2O_2NO_3 + H_2WO_4 \rightarrow Bi_2WO_6 + H^+ + NO_3^- + H_2O \quad (3)$$

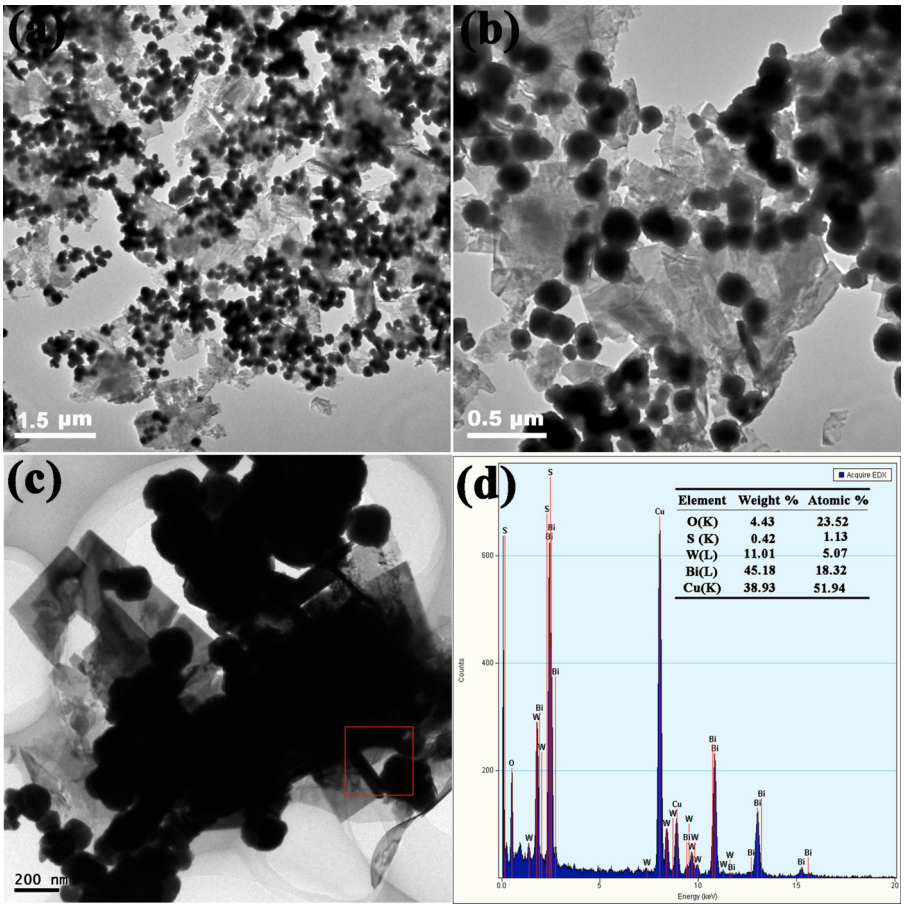

Fig. 3. TEM images (a–c) with various resolutions of WS_2-BWO and (d) EDS analysis of the selected field with red wireframe in (c).

When the pH value is higher than that of 10.5, the reaction is illustrated as below:

$$Bi_2O_2NO_3 + {WO_4}^{2-} + OH^- \rightarrow Bi_{3.84}W_{0.16}O_{6.24} + {NO_3}^- + H_2O \quad (4)$$

With introducing the few layered WS_2 and adjusting the pH value of 10.5, the Bi^{3+} ions interact electrostatically with WS_2 to form Bi^{3+}-WS_2 complexes, and then react in the hydrothermal process as below:

$$Bi^{3+}\text{-}WS_2 + H_2WO_4 + {WO_4}^{2-} + OH^- \rightarrow WS_2\text{-}Bi_2WO_6/Bi_{3.84}W_{0.16}O_{6.24} + H_2O \quad (5)$$

The above reaction formulas suggest that a low pH value is favorable for the formation of the Bi_2WO_6 phase. If the pH value increases gradually, the $Bi_2O_2(OH)NO_3$ will react with OH^- and ${WO_4}^{2-}$ to form the the $Bi_{3.84}W_{0.16}O_{6.24}$ phase gradually. Therefore, at the critical pH value, the Bi^{3+}-WS_2 complexes can simultaneously react with H_2WO_4 and ${WO_4}^{2-}$ to obtain a heterostructured WS_2-Bi_2WO_6/$Bi_{3.84}W_{0.16}O_{6.24}$composite.

3.3. Photocatalytic performance

The photocatalytic performance of the samples was evaluated using the degradation of organic dyes RhB under visible-light irradiation as a model reaction. As shown in Figs. 7a and S4, a blank test (RhB without any catalyst) reveals that the RhB is stable under visible light irradiation. The photodegradation of RhB with WS_2-BWO in the dark is similar to that of the blank test. The physical mixture of BWO and the few layered WS_2 (the same ratio in preparation of WS_2-BWO) show a similar photocatalytic activity of BWO, which are both obviously worse than that of WS_2-BWO and (B)WS_2-BWO. As for the samples of WS_2-Bi_2WO_6, WS_2-$Bi_{3.84}W_{0.16}O_{6.24}$, Bi_2WO_6, and $Bi_{3.84}W_{0.16}O_{6.24}$, their photocatalytic performances are all inferior to that of WS_2-BWO. In order to well compare the photodegradation rate of RhB with different catalysts, the kinetic experiments were done. As shown in Fig. S5 and Table S1, the Rate constant for photodegradation of RhB over the samples of WS_2-BWO, (B)WS_2-Bi_2WO_6, BWO and the physical mixture of BWO and the few layered WS_2 is 0.04301, 0.02968, 0.01489, and 0.01539 min^{-1}, respectively. Hence, the better performance is considered to be due to the formation of chemical bonding between BWO and tungsten sulfide among the heterostructured composites. However, compared with (B)WS_2-BWO, the few layered WS_2-BWO composite shows much better photocatalytic performance under visible light irradiation (Fig. S6), which is attributed to the two-dimensional structure of WS_2 with special properties and the matching energy band structure between WS_2 and BWO for efficient separation of photogenernated electron–hole pairs.

In order to check the stability and efficiency of the photocatalytic performance of the WS_2-BWO composite for further applications, repetitive runs of photocatalytic degradation of RhB under visible light are carried out. As shown in Fig. 7b, after four of repetitive runs, the photocatalytic performance nearly remains unchanged, which indicates that the WS_2-BWO composite exhibits good stability.

Active species trapping experiments are further carried out to determine the major reactive species accounting for the photocatalytic degradation of RhB over the few layered WS_2-BWO under visible irradiation, including isopropanol (2 mM) for $^{\bullet}OH$, sodium oxalate (2 mM) for h^+, and benzoquinone (2 mM) for ${}^{\bullet}O_2^-$.

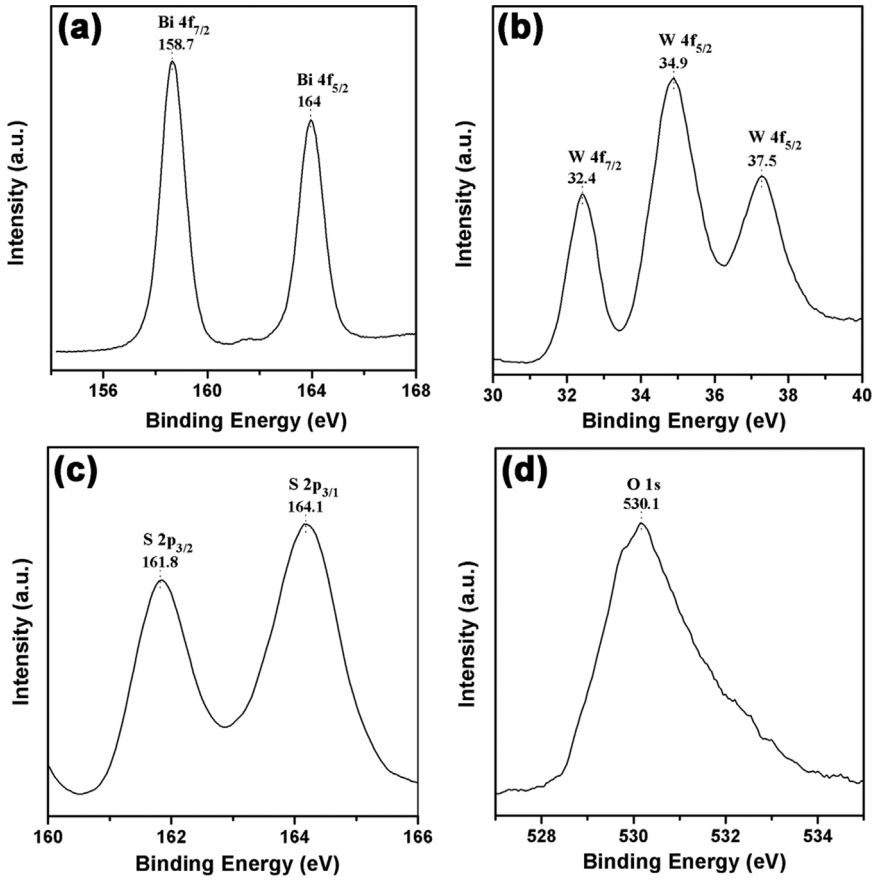

Fig. 4. XPS scans of (a) Bi 4f, (b) W4f, (c) S2p, and (d) O 1sof the as-prepared WS_2-BWO.

As shown in Fig. 8, the impact degree of scavengers on photodegradation of RhB from high to low is benzoquinone, sodium oxalate and isopropanol, respectively. The results clearly indicate that the $^{\bullet}O_2^-$ plays a leading role in the degradation process, the second is h^+, and the $^{\bullet}OH$ contributes slightly. When O_2 was bubbled to enrich the oxygen in the solution, there is a significant increase of RhB degradation. This phenomenon further reveals that the reaction of molecular oxygen with photogenerated electrons for the generation of $^{\bullet}O_2^-$ is important for RhB degradation over WS_2-BWO.

3.4. Photocatalytic enhancement mechanism

As well known, few-layered WS_2 can act as an electron acceptor and a transporter due to its 2D π-conjugation structure. Thus the typical electrochemical impedance spectra (EIS) of the as-prepared catalysts were investigated. As shown in Fig. S7, the semicircles in Nyquist plots of the samples have an order (WS_2-BWO < WS_2-Bi_2WO_6 < WS_2-$Bi_{3.84}W_{0.16}O_{6.24}$ < Bi_2WO_6 < BWO < $Bi_{3.84}W_{0.16}O_{6.24}$). Furthermore, the photocurrent responses of the as-prepared samples were inves-

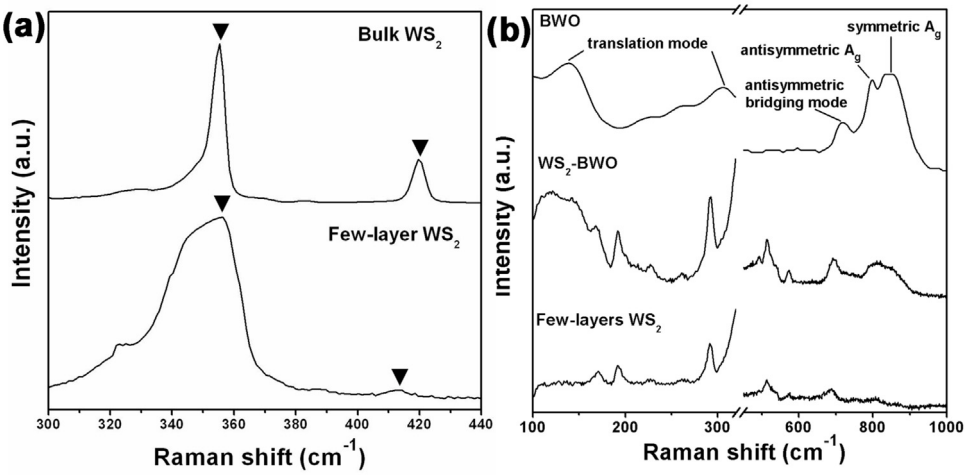

Fig. 5. Raman spectra of bulk WS_2 and few-layer WS_2 (a); BWO and WS_2-BWO (b).

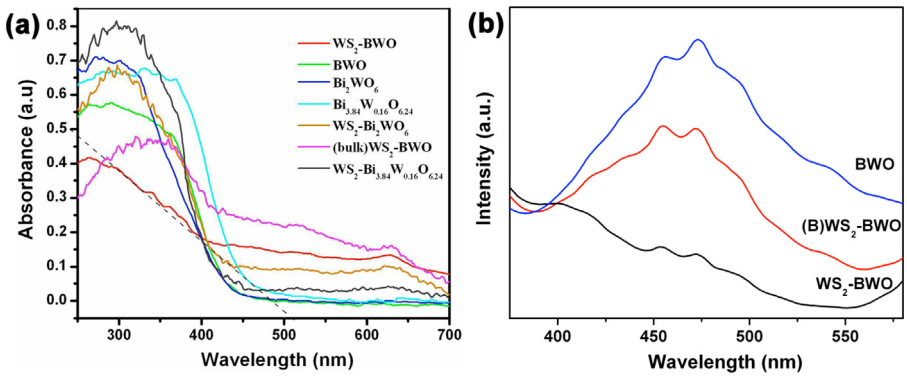

Fig. 6. (a) The UV–vis diffuse reflectance spectrum of the as-prepared WS_2-BWO, BWO, Bi_2WO_6, WS_2-Bi_2WO_6, WS_2-$Bi_{3.84}W_{0.16}O_{6.24}$, (bulk)$WS_2$-BWO, and $Bi_{3.84}W_{0.16}O_{6.24}$ samples; (b) Photoluminescence spectra of WS_2-BWO, (B) WS_2-BWO and BWO samples.

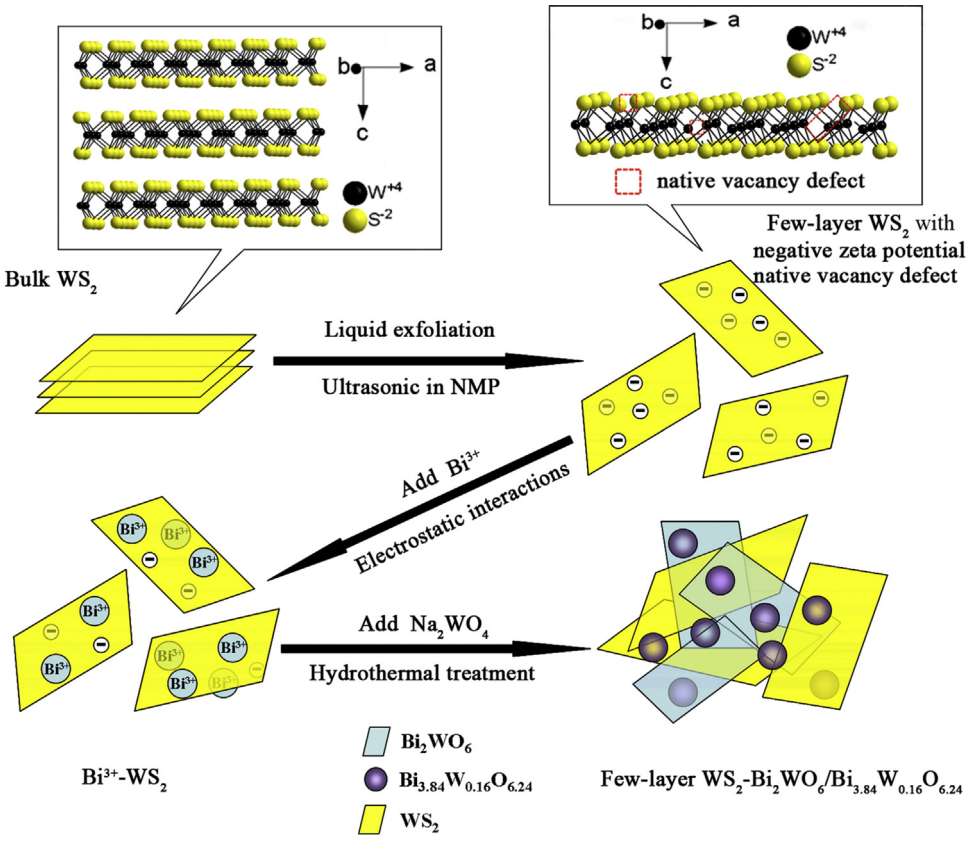

Scheme 1. Formation mechanism of the few-layer WS_2-BWO composite.

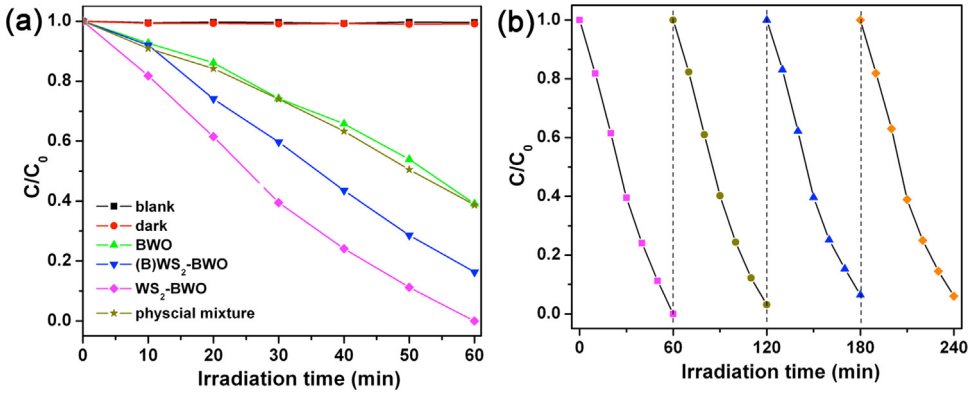

Fig. 7. (a) Photodegradation of RhB over several different samples under visible irradiation. (b) Repetitive runs of the photodegradation of RhB over the few layered WS_2-BWO under visible irradiation.

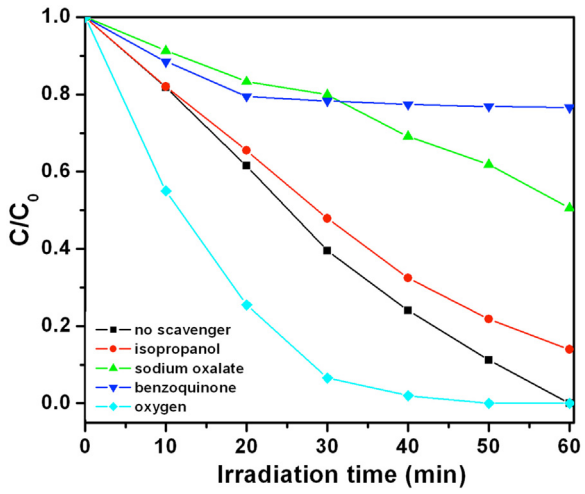

Fig. 8. Effects of different scavengers and oxygen on photodegradation of RhB over the few-layer WS_2-BWO under visible irradiation.

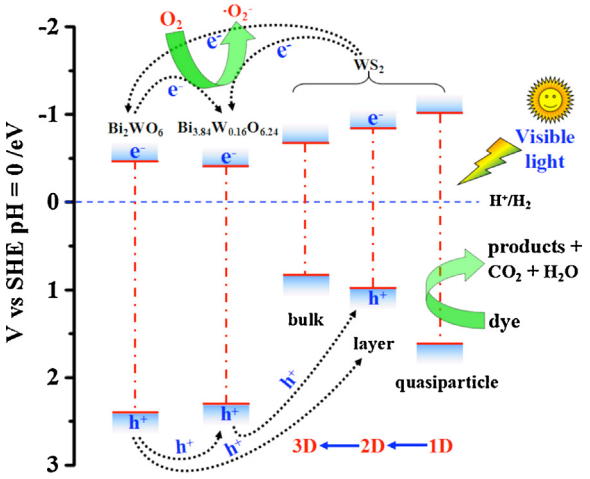

Fig. 9. Schematic illustration of the energy band positions and photocatalytic process of the WS_2-BWO composite.

tigated for several on-off cycles under visible light irradiation. As shown in Fig. S8, the intensity of fast photocurrent responses shows an obvious order (WS_2-BWO > WS_2-Bi_2WO_6 > Bi_2WO_6 > WS_2-$Bi_{3.84}W_{0.16}O_{6.24}$ > BWO > $Bi_{3.84}W_{0.16}O_{6.24}$). These results indicate that the few-layered WS_2-BWO possesses the best efficient among the as-prepared samples in terms of interfacial charge transfer as well as separation of photogenerated electrons and holes.

Based on the above results, the proposed mechanism for photodegradation of RhB dye over the few layered WS_2-BWO composite is displayed in Fig. 9. Table S2 and Fig. S9 show the energy levels of conduction and valence band edges *vs* standard hydrogen electrode (SHE, at pH 0) for Bi_2WO_6, $Bi_{3.84}W_{0.16}O_{6.24}$, and WS_2 with various dimensions (detailed description shown in Supporting Information). Under the irradiation of visible light, electron and hole pairs are produced in the conduction band (CB) and valence band (VB), respectively. As for the BWO sample, the photogenerated electrons would transfer from the CB of Bi_2WO_6 to that of $Bi_{3.84}W_{0.16}O_{6.24}$, whereas the photogenerated holes would transfer from the VB of Bi_2WO_6 to that of $Bi_{3.84}W_{0.16}O_{6.24}$, respectively. These would result in the recombination of electron–hole pairs. Introduced with WS_2 (bulk or few-layer), the composites exhibit a better photocatalytic performance due to the matching energy levels. The photogenerated electrons transfer from the CB of Bi_2WO_6 to that of $Bi_{3.84}W_{0.16}O_{6.24}$, meanwhile, the photogenerated holes transfer from the VB of Bi_2WO_6 or $Bi_{3.84}W_{0.16}O_{6.24}$ to that of WS_2, which efficiently separate the electron–hole pairs and suppress the recombination. And another pathway of electron–hole pairs' separation will occur between Bi_2WO_6 and few-layer WS_2 due to the good contact and the matched energy structure. The photogenerated electrons transfer from the CB of WS_2 to that of Bi_2WO_6, and the photogenerated holes transfer from the VB of Bi_2WO_6 to that of WS_2, which efficiently separate the electron-hole pairs. In addition, because the two-dimensional (2D) WS_2 possesses distinctive electronic, optical, catalytic properties, especially a faster charge mobility than that of one-dimensional (1D) or three-dimensional (3D) structure [16,59–61], the few layered WS_2-BWO shows a better photocatalytic performance compared with bulk WS_2-BWO. Moreover, the few layered WS_2 nanosheets can combine with the Bi_2WO_6 nanosheets and $Bi_{3.84}W_{0.16}O_{6.24}$ nanoparticles more uniformly and intimately, which facilitates the effective interaction between them and provide more active sites for the photocatalytic process. The above factors are the main reasons that lead to the enhanced activity of the few layered WS_2-BWO composite.

4. Conclusions

In summary, we have developed a novel electrostatically driven hydrothermal approach to synthesize the few layered WS_2-Bi_2WO_6/$Bi_{3.84}W_{0.16}O_{6.24}$ heterostructured composite with an enhanced photocatalytic performance and good stability. The 2D few layered WS_2 nanosheets firstly act as a substrate to combine with the bismuth tungstate composite to obtain a novel heterostructured WS_2-Bi_2WO_6/$Bi_{3.84}W_{0.16}O_{6.24}$. A possible formation mechanism was proposed. The photocatalytic mechanism was put forward to explain the effectiveness of interfacial charge transfer and the photocatalytic efficiency of the ternary heterostructured composites. Overall, the present work not only opens up an avenue to the syntheses of few layered WS_2 combined with composites to form heterostructured photocatalysts with excellent activity for environmental treatment, but also promotes the investigation of a wider variety of layered TMDs based composites.

Acknowledgements

We gratefully acknowledge the financial support of the NSF of China (51238002, 51272099, 51378246, and 20801026), the NSF of Jiangxi Province (KJLD12002 and 20114BAB203005), and the Foundation of State Key Laboratory of Structural Chemistry (20100015).

Appendix A. Supplementary data

Supplementary data associated with this article can be found, in the online version, at http://dx.doi.org/10.1016/j.apcatb.2015.05.031

References

[1] K.S. Novoselov, A.K. Geim, S.V. Morozov, D. Jiang, Y. Zhang, S.V. Dubonos, I.V. Grigorieva, A.A. Firsov, Science 306 (2004) 666–669.
[2] H.S. Chang, H.K. Wu, Energy Environ. Sci. 6 (2013) 3483–3507.
[3] M. Chhowalla, H.S. Shin, G. Eda, L.J. Li, K.P. Loh, H. Zhang, Nat. Chem. 5 (2013) 263–275.
[4] X. Huang, Z.Y. Zeng, H. Zhang, Chem. Soc. Rev. 42 (2013) 1934–1946.
[5] M.S. Xu, T. Liang, M.M. Shi, H.Z. Chen, Chem. Rev. 113 (2013) 3766–3798.
[6] J. Yang, H.S. Shin, J. Mater. Chem. 2 (2014) 5979–5985.
[7] Z.Y. Yin, H. Li, H. Li, L. Jiang, Y.M. Shi, Y.H. Sun, G. Lu, Q. Zhang, X.D. Chen, H. Zhang, ACS Nano 6 (2012) 74–80.
[8] O. Lopez-Sanchez, D. Lembke, M. Kayci, A. Radenovic, A. Kis, Nat. Nanotechnol. 8 (2013) 497–501.
[9] Y. Zhao, X. Luo, H. Li, J. Zhang, P.T. Araujo, C.K. Gan, J. Wu, H. Zhang, S.Y. Quek, M.S. Dresselhaus, Q. Xiong, Nano Lett. 13 (2013) 1007–1015.
[10] A.L. Elias, N. Perea-Lopez, A. Castro-Beltran, A. Berkdemir, R.T. Lv, S.M. Feng, A.D. Long, T. Hayashi, Y.A. Kim, M. Endo, H.R. Gutierrez, N.R. Pradhan, L.

Balicas, T.E.M. Houk, F. Lopez-Urias, H. Terrones, M. Terrones, ACS Nano 7 (2013) 5235–5242.
[11] H.L. Li, X.D. Duan, X.P. Wu, X.J. Zhuang, H. Zhou, Q.L. Zhang, X.L. Zhu, W. Hu, P.Y. Ren, P.F. Guo, L. Ma, X.P. Fan, X.X. Wang, J.Y. Xu, A. Pan, X.F. Duan, J. Am. Chem. Soc. 136 (2014) 3756–3759.
[12] G. Eda, H. Yamaguchi, D. Voiry, T. Fujita, M.W. Chen, M. Chhowalla, Nano Lett. 11 (2011) 5111–5116.
[13] R.R. Chianelli, M.H. Sciadati, M.P. De la Rosa, G. Berhault, J.P. Wilcoxon, R. BearDen, B.L. Abrams, Catal. Rev. : Sci. Eng. 48 (2006) 1–41.
[14] M.S. Whittingham, Chem. Rev. 104 (2004) 4271–4302.
[15] L. Rapoport, N. Fleischer, R. Tenne, J. Mater. Chem. 15 (2005) 1782–1788.
[16] B. Radisavljevic, A. Radenovic, J. Brivio, V. Giacometti, A. Kis, Nat. Nanotechnol. 6 (2011) 147–150.
[17] D. Voiry, H. Yamaguchi, J.W. Li, R. Silva, D.C.B. Alves, T. Fujita, M.W. Chen, T. Asefa, V.B. Shenoy, G. Eda, M. Chhowalla, Nat. Mater. 12 (2013) 850–855.
[18] Z.Z. Wu, B.Z. Fang, A. Bonakdarpour, A. Sun, D.P. Wilkinson, D.Z. Wang, Appl. Catal. B: Environ. 125 (2012) 59–66.
[19] S.X. Min, G.X. Lu, J. Phys. Chem. C 116 (2012) 25415–25424.
[20] Q.J. Xiang, J.G. Yu, M. Jaroniec, J. Am. Chem. Soc. 134 (2012) 6575–6578.
[21] Y. Zhou, K. Vuille, A. Heel, G.R.Z. Patzke, Anorg. Allg. Chem. 635 (2009) 1848–1855.
[22] Y.Y. Li, J.P. Liu, X.T. Huang, Nanoscale Res. Lett. 3 (2008) 365–371.
[23] S.W. Liu, J.G. Yu, J. Solid State Chem. 181 (2008) 1048–1055.
[24] C.X. Xu, X. Wei, Z.H. Ren, Y. Wang, G. Xu, G. Shen, G.R. Han, Mater. Lett. 63 (2009) 2194–2197.
[25] L.S. Zhang, W.Z. Wang, Z.G. Chen, L. Zhou, H.L. Xu, W. Zhu, J. Mater. Chem. 17 (2007) 2526–2532.
[26] M. Shang, W.Z. Wang, H.L. Xu, Cryst. Growth Des. 9 (2009) 991–996.
[27] L.S. Zhang, W.Z. Wang, L. Zhou, H.L. Xu, Small 3 (2007) 1618–1625.
[28] Q.C. Xu, D.V. Wellia, Y.H. Ng, R. Amal, T.T.Y. Tan, J. Phys. Chem. C 115 (2011) 7419–7428.
[29] X.N. Li, R.K. Huang, Y.H. Hu, Y.J. Chen, W.J. Liu, R.S. Yuan, Z.H. Li, Inorg. Chem. 51 (2012) 6245–6250.
[30] Z.J. Zhang, W.Z. Wang, L. Wang, S.M. Sun, ACS Appl. Mater. Interfaces 4 (2012) 593–597.
[31] Q. Xiao, J. Zhang, C. Xiao, X.K. Tan, Catal. Commun. 9 (2008) 1247–1253.
[32] F. Duan, Y. Zheng, M.Q. Chen, Appl. Surf. Sci. 257 (2011) 1972–1978.
[33] E.P. Gao, W.Z. Wang, M. Shang, J.H. Xu, Phys. Chem. Chem. Phys. 13 (2011) 2887–2893.
[34] Y.L. Min, K. Zhang, Y.C. Chen, Y.G. Zhang, Sep. Purif. Technol. 85 (2012) 98–105.
[35] S.X. Li, J. Chen, F.Y. Zheng, Y.C. Li, F.Y. Huang, Nanoscale 5 (2013) 12150–12155.
[36] S.X. Li, J. Chen, F.Y. Zheng, Y.C. Li, F.Y. Huang, Nanoscale 5 (2013) 12150–12155.
[37] Y. Liu, Q. Li, S.A. Gao, J.K. Shang, CrystEngComm 16 (2014) 7493–7501.
[38] J.P. Zou, S.L. Luo, L.Z. Zhang, J. Ma, S.L. Lei, L.S. Long, X.B. Luo, Y. Luo, G.S. Zeng, C.T. Au, Appl. Catal. B: Environ. 140 (2013) 608–618.
[39] J.P. Zou, J. Ma, Q. Huang, S.L. Luo, J. Yu, X.B. Luo, W.L. Dai, J. Sun, G.C. Guo, C.T. Au, S.L. Suib, Appl. Catal. B: Environ. 156–157 (2014) 447–455.
[40] S. Chen, X. Yu, H. Zhang, W. Liu, J. Hazard. Mater. 180 (2010) 735–740.
[41] X. Wang, Q. Xu, M.R. Li, S. Shen, X.L. Wang, Y.C. Wang, Z.C. Feng, J.Y. Shi, H.X. Han, C. Li, Angew. Chem. Int. Ed. 51 (2012) 13089–13092.
[42] J.N. Coleman, M. Lotya, A. O'Neill, D. Bergin, P.J. King, U. Khan, K. Young, A. Gaucher, S. De, R.J. Smith, Science 331 (2011) 568–571.
[43] Y.D. Liu, L. Ren, X. Qi, L.W. Yang, G.L. Hao, J. Li, X.L. Wei, J.X. Zhong, J. Alloys Compd. 571 (2013) 37–42.
[44] V. Stengl, J. Henych, Nanoscale 5 (2013) 3387–3394.
[45] D. Gopalakrishnan, D. Damien, M.M. Shaijumon, ACS Nano 8 (2014) 5297–5303.
[46] Y.M. Cui, H.Q. Li, W.S. Hong, S.H. Fan, L.J. Zhu, Powder Technol. 247 (2013) 151–160.
[47] C.Y. Wang, L.Y. Zhu, C. Song, G.Q. Shan, P. Chen, Appl. Catal. B: Environ. 105 (2011) 229–236.
[48] S.S. Xu, X.M. Gao, J.Y. Sun, D. Jiang, F. Zhou, W.M. Liu, L.J. Weng, Appl. Surf. Sci. 288 (2014) 15–25.
[49] P.C. Yen, Y.S. Huang, K.K. Tiong, J. Phys. -Condens. Mat. 16 (2004) 2171–2180.
[50] N.T. McDevitt, J.S. Zabinski, M.S. Donley, Thin Solid Films 240 (1994) 76–81.
[51] T. Sekine, T. Nakashizu, K. Toyoda, K. Uchinokura, E. Matsuura, Solid State Commun. 35 (1980) 371–373.
[52] S. Sugai, T. Ueda, K. Murase, J. Physiol. (Paris) 42 (1981) 320–322.
[53] C. Lee, H. Yan, L.E. Brus, T.F. Heinz, J. Hone, ACS Nano 4 (2010) 2695–2700.
[54] G. Cunningham, M. Lotya, C.S. Cucinotta, S. Sanvito, S.D. Bergin, R. Menzel, M.S.P. Shaffer, J.N. Coleman, ACS Nano 6 (2012) 3468–3480.
[55] D.Y. Kim, S.J. Kim, M.K. Yeo, I.G. Jung, M. Kang, J. Chem. Eng. 26 (2009) 261–264.
[56] M. Crane, R.L. Frost, P.A. William, J. Raman Spectrosc. 33 (2002) 62–66.
[57] J. Zhang, Z.H. Huang, Y. Xu, F.Y. Kang, J. Am. Ceram. Soc. 96 (2013) 1562–1569.
[58] K.G. Zhou, N.N. Mao, H.X. Wang, Y. Peng, H.L. Zhang, Angew. Chem. Int. Ed. 50 (2011) 10839–10842.
[59] X. Zong, H. Yan, G. Wu, G. Ma, F. Wen, L. Wang, C. Li, J. Am. Chem. Soc. 130 (2008) 7176–7177.
[60] R.V. Kasowski, Phys. Rev. Lett. 30 (1973) 1175–1178.
[61] L.F. Mattheis, Phys. Rev. Lett. 30 (1973) 784–787.